RSC Advances

PAPER

View Article Online
View Journal | View Issue

Cite this: *RSC Adv.*, 2019, **9**, 36171

A molecular understanding of the interaction of typical aromatic acids with common aerosol nucleation precursors and their atmospheric implications†

Hetong Wang,[ab] Xianwei Zhao,[b] Chenpeng Zuo,[b] Xiaohui Ma,[b] Fei Xu,*[ab] Yanhui Sun[c] and Qingzhu Zhang[b]

Aromatic acids, which are generated from numerous anthropogenic emissions and secondary transformations, have been considered to play a crucial role in new particle formation. In this study, we performed theoretical calculations at the PW91PW91/6-311++G(3df,3pd) level to investigate the interaction between typical aromatic acids namely benzoic acid (BA), phenylacetic acid (PAA), phthalic acid (PA), isophthalic acid (mPA), and terephthalic acid (PTA) and common atmospheric nucleation precursors namely sulfuric acid (SA), water (H_2O), ammonia (NH_3), methylamine (MA), dimethylamine (DMA), and trimethylamine (TMA). The geometric analysis, Gibbs free energy analysis, OH/NH-stretching vibrational frequency calculation, and atoms in molecules (AIM) analysis were conducted to determine the interactions in the complexes. The heterodimers formed a six to eight membered ring through four types of hydrogen bond, and the bond strength could be ranked in descending order: SO–H···O > O–H···O/N > N–H···O. The BA/PAA/mPA/PTA–SA complexes had the lowest Gibbs free energy values. PA was more likely to interact with NH_3 or amines rather than SA due to an intra-molecular hydrogen bond. Additionally, the aromatic acids have similar ability to interact with SA and NH_3 as monocarboxylic/dicarboxylic acid. The formation potential of the heterodimers from aromatic acids with common nucleation precursors in ambient atmosphere was investigated.

Received 14th September 2019
Accepted 29th October 2019

DOI: 10.1039/c9ra07398a

rsc.li/rsc-advances

1. Introduction

Atmospheric aerosols can substantially increase the concentration of cloud condensation nuclei (CCN) and may affect the Earth's climate.[1–4] Gas-phase nucleation is a key research area, and new particle formation (NPF) through nucleation is a vital source of atmospheric aerosols.[5] However, the NPF process in the atmosphere, which includes multiple components, is highly complex. Although several investigations have been conducted on this process, the precise mechanisms and substances involved at the molecular level are still not adequately understand.

To explain the nucleation mechanisms, binary sulfuric acid (SA)–water (H_2O), ternary SA–H_2O–ammonia (NH_3),[6] and ion-induced nucleation,[7,8] and nucleation enhanced by organic compounds have been proposed.[9] The importance of SA in new particle formation has been widely investigated, and numerous studies have proven that SA is a crucial atmospheric nucleating species.[1,10] However, a gaseous SA concentration of more than 10^5 molecules per cm^3 is required to observe NPF in the atmosphere.[11,12] Therefore, the vital role of organic species in NPF has attracted considerable attention. On the basis on the experimental methods, research has been proven that atmospheric aerosol particles indeed contain a large amount of organic compounds.[13–15] Experimental results obtained from such research have shown that organic acids play a key role in the initial growth stage of newly nucleated embryos, and this process is crucial for the subsequent step of particle growth through adsorption or heterogeneous reactions of other organic vapors. Additionally, quantum chemical calculations have demonstrated that an aromatic acid–SA cluster can reduce the nucleation barrier and that a binary SA–H_2O nucleation system can be enhanced by sub-ppb levels of organic acids simultaneously.[9]

[a]*Shenzhen Research Institute of Shandong University, Shenzhen 518057, P. R. China. E-mail: xufei@sdu.edu.cn; Fax: +86-532-5863198*

[b]*Environment Research Institute, Shandong University, Qingdao 266237, P. R. China*

[c]*College of Environment and Safety Engineering, Qingdao University of Science & Technology, Qingdao 266042, P. R. China*

† Electronic supplementary information (ESI) available: The minimum energy configurations of monomer. Geometric parameters of the O–H···O intra-molecular hydrogen bonds in the PA-containing complexes. Intra-molecular bonded OH-stretching wavenumbers and red shifts of PA-containing complexes. Atoms in molecules (AIM) parameter analysis for the intra-molecular hydrogen bonds of PA-containing complexes. Cartesian coordinates of the minimum energy configurations. See DOI: 10.1039/c9ra07398a

Aromatic acids belong to a group of organic acids, which include monocarboxylic acids and dicarboxylic acids. Benzoic acid (BA) is a typical aromatic monocarboxylic acid, that is generated from numerous anthropogenic emissions, such as motor vehicles and fuel burning.[16] BA is also a secondary product of the photochemical degradation of aromatic hydrocarbons.[17] Phthalic acid (PA), isophthalic acid (mPA), and terephthalic acid (PTA) are aromatic dicarboxylic acids, that have been extensively discovered in the ambient atmosphere. PA can be emitted from the oxidation of polycyclic aromatic hydrocarbons (PAHs), including benz[*a*]anthracene and naphthalene.[18–21] It can also be generated from the burning of biomass, combustion of coal, and exhaust of diesel engines.[22] Furthermore, mPA and PTA are primarily produced from the direct emission of automobile exhaust and biomass burning; mPA can also be derived from secondary aerosols.[23] Liu and Zeng demonstrated that aromatic acids may be transformed by interacting with common atmospheric oxidants (O_3, Cl, NO_3, and OH radicals) through heterogeneous or homogeneous reactions.[24] Zhang *et al.* detected five types of aromatic acids in $PM_{2.5}$ in the northern suburb of Nanjing during winter; the average total concentration of the detected aromatic acids was (50.01 ± 16.05) ng m^{-3}, and the average concentrations of PA, mPA and PTA were (8.14 ± 3.34), (1.08 ± 0.43), and (34.54 ± 12.79) ng m^{-3}, respectively.[23] In addition, a study reported the detection of aromatic dicarboxylic acids in the Los Angeles ambient atmosphere.[25] Zhang *et al.* verified that the nucleation rates of SA–H_2O systems can be extensively reinforced by the presence of a small quantity of aromatic organic acids.[9] Xu and Zhang verified that PA can interact with sulfuric acid and ammonia to playing a key role in aerosol nucleation.[26] Therefore, further investigation regarding the role of aromatic acids in nucleation is worthwhile.

In the present study, we investigated the interaction of five aromatic acids namely BA, PAA, PA, mPA, and PTA with common atmospheric aerosol nucleation precursors (SA, H_2O, NH_3, methylamine (MA), dimethylamine (DMA), and trimethylamine (TMA)) at the molecular level. By using density functional theory (DFT) methods, we conducted theoretical calculations of these complexes to determine geometric parameters, binding energies and Gibbs free energies. Subsequently, we used atoms in molecules analysis (AIM) to determine the electronic densities and hydrogen bonding interactions in the complexes.[27,28]

2. Computational methods

The chemical geometries for the investigated compounds were determined by an artificial bee colony algorithm software called ABCluster (artificial bee colony algorithm for cluster), which is used for the global optimization of atomic and molecular clusters.[29,30] ABCluster is a useful tool for determining the geometry of a cluster with the lowest energy. Density functional theory (DFT) calculations were performed using the Gaussian 09 package.[31] First, up to 1000 initially guessed structures were auto-generated and pre-optimized by the semiempirical PM6 method using ABCluster. Second, up to 100 conformations with relatively low energies were selected from the 1000 structures and subsequently optimized at the B3LYP/6-31*g*(d,p) level; their corresponding vibrational frequencies were calculated at the same level. Finally, the PW91PW91 density functional method with a 6-311++G(3df,3pd) basis set was employed to further reoptimize the 10 most stable of the 100 optimized structures in order to derive the global minimum structure. Their corresponding thermal free energies (ΔG), thermal enthalpies (ΔH), zero-point vibrational energy (ZPVE), and binding energy (BE) were also obtained at the PW91PW91/6-311++G(3df,3pd) level. The BEs of the complexes were corrected with ZPVEs. Several basic clusters formation has been investigated at the M06-2X/6-311++G(3df,3pd) level of theory and recommended to be a more reliable method for predicting the formation of binary and ternary clusters.[32–34] The comparison of Gibbs free energy calculated by two different DFT theories in this study was shown in Table 2. The differences between the Gibbs free energies calculated at PW91PW91/6-311++G(3df,3pd) and M06-2X/6-311++G(3df,3pd) were within 2.0 kcal mol^{-1}, which proves the consistency of the two methods. In this study, the analysis of configurations and energies was carried out at PW91PW91/6-311++G(3df,3pd) level of theory.

To describe the strength and various classes of the hydrogen bonds, we performed a topological analysis of the charge density by using the AIM2000 program package through atoms in molecules (AIM) theory. AIM theory has been recognized as a powerful method for obtaining a relatively clear understanding of hydrogen bonding interactions.[27,28] Additionally, electron density properties at the bond critical point (BCP), bond critical point charge density $\rho(r)$, and Laplacian of charge density $\nabla^2\rho(r)$ serve as an indicator to describe hydrogen bonding.[35]

3. Results and discussion

3.1 Geometric analysis

The geometries of SA, H_2O, NH_3, MA, DMA, and TMA as well as those of BA, PAA, PA, mPA, and PTA were optimized at the PW91PW91/6-311++G(3df,3pd) level using the Gaussian 09 package. Several possible configurations of the complexes were found, but only the most stable structures of the clusters are discussed in this paper. The minimum energy configurations of monomer are displayed in Fig. S1.† The optimized structures of the heterodimers are shown in Fig. 1, and the geometric parameters of the clusters are presented in Table 1. The intramolecular O–H···O hydrogen bonds of PA-containing complexes are displayed in Table S1.† Cartesian coordinates of the minimum energy configurations are shown in Table S4.†

Aromatic acids and SA formed an eight-membered ring through a SO–H···O and a CO–H···O hydrogen bonds. For the PA–SA complex, the carboxyl group formed an intra-molecular CO–H···O hydrogen bond with a second carboxyl group of PA apart from the eight-membered ring. For the aromatic acid–NH_3/MA/DMA complexes, the carboxyl group in the aromatic acids and the nitrogen atom in NH_3/MA/DMA formed a CO–H···N hydrogen bond, and the N–H···O hydrogen bond was formed between the hydrogen atom in NH_3/MA/DMA and the oxygen

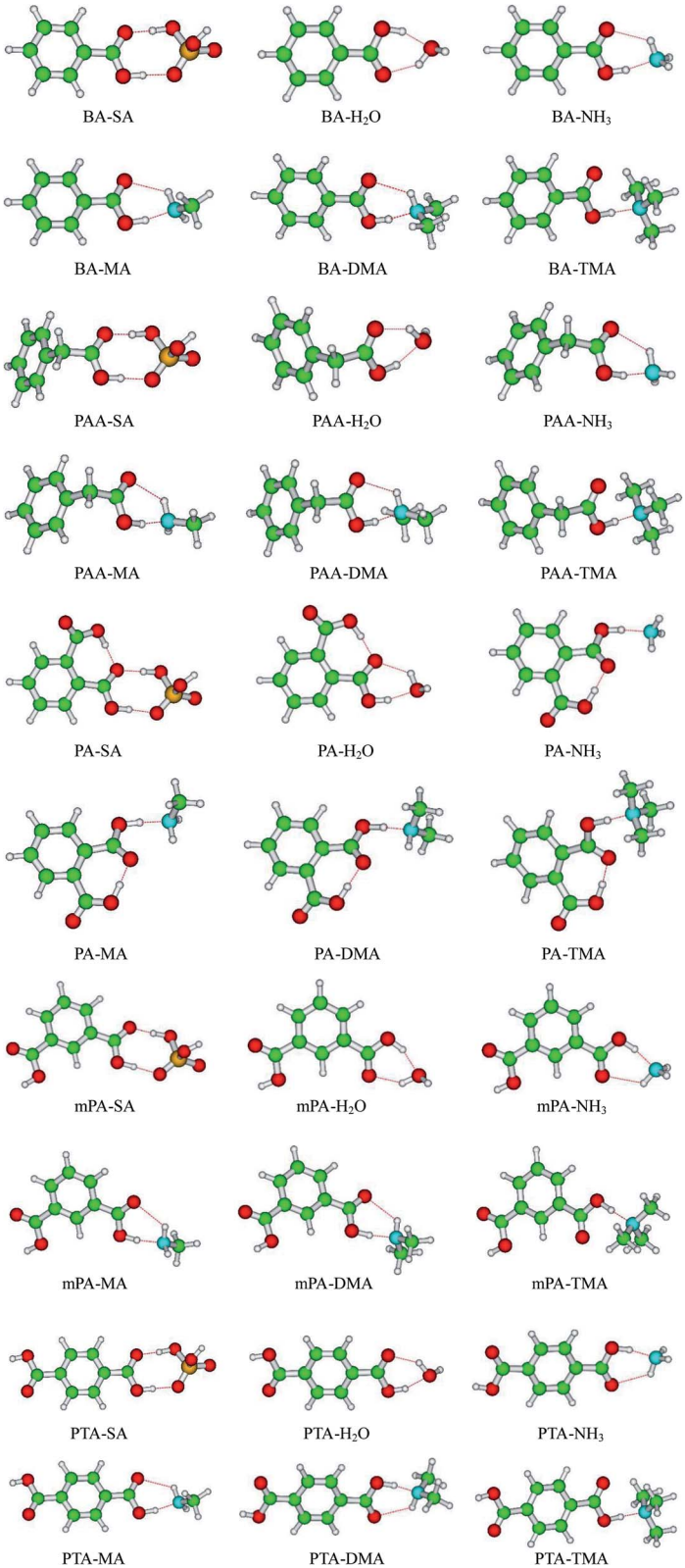

Fig. 1 Geometries of aromatic acid-containing complexes calculated at the PW91PW91/6-311++G(3df,3pd) level. Green, yellow, blue, white, and red balls denote C, S, N, H, and O atoms, respectively.

atom in the carboxyl of the aromatic acid. All of these hetero-dimers formed a six-membered ring. For the aromatic acid–TMA cluster, a seven-membered ring was produced through a CO–H···N hydrogen bond and a C–H···O hydrogen bond. PA contained one more intra-molecular hydrogen bond compared with the other aromatic acids. The aromatic acids formed a six-

Table 1 Geometric parameters of the SO–H···O, O–H···O/N, and N–H···O hydrogen bonds in aromatic acid-containing complexes derived at the PW91PW91/6-311++G(3df,3pd) level. Angles are given in degrees (°); lengths and distances are given in angstrom (Å)

	SO–H···O				O–H···O/N				N–H···O		
Conformer	$\Delta r(OH)^a$	$r(HB)^b$	$\theta(HB)^c$	$d(O\cdots O)^d$	$\Delta r(OH)^a$	$r(HB)^b$	$\theta(HB)^c$	$d(O\cdots O)^d$	$\Delta r(NH)^e$	$r(HB)^b$	$\theta(HB)^c$
BA–SA	0.0863	1.4431	175.5	2.5036	0.0321	1.6380	178.4	2.6457			
BA–H_2O					0.0297/0.0222	1.7147/1.8450	157.8/143.7	2.6728/2.7073			
BA–NH_3					0.0499	1.6789	168.1		0.0042	2.2890	123.6
BA–MA					0.0630	1.6329	169.3		0.0052	2.3061	122.7
BA–DMA					0.0721	1.6072	169.8		0.0063	2.2809	123.9
BA–TMA					0.0727	1.6096	179.3				
PAA–SA	0.0818	1.4577	175.8	2.5139	0.0321	1.6415	178.9	2.6504			
PAA–H_2O					0.0293/0.0215	1.7198/1.8582	157.2/143.3	2.6758/2.7168			
PAA–NH_3					0.0499	1.6792	167.8		0.0040	2.3140	122.9
PAA–MA					0.0634	1.6314	169.1		0.0051	2.3257	122.3
PAA–DMA					0.0724	1.6054	169.8		0.0060	2.3136	122.8
PAA–TMA					0.0729	1.6071	179.2				
PA–SA	0.0493	1.5675	177.3	2.5921	0.0333	1.6269	170.0	2.6360			
PA–H_2O					0.0348/0.0122	1.6610/2.0343	163.4/131.2	2.6460/2.7797			
PA–NH_3					0.0667	1.6082	174.5	2.5221			
PA–MA					0.0911	1.5434	175.2	2.5175			
PA–DMA					0.1158	1.4880	175.5	2.5155			
PA–TMA					0.1264	1.4699	177.2	2.5150			
mPA–SA	0.0786	1.4621	175.9	2.5159	0.0330	1.6333	178.7	2.6420			
mPA–H_2O					0.0310/0.0210	1.7038/1.8633	160.0/142.2	2.6641/2.7135			
mPA–NH_3					0.0537	1.6626	168.7		0.0038	2.3267	121.6
mPA–MA					0.0684	1.6129	170.2		0.0047	2.3529	120.4
mPA–DMA					0.0794	1.5824	170.9		0.0059	2.3326	121.5
mPA–TMA					0.0804	1.5837	178.7				
PTA–SA	0.0775	1.4661	175.9	2.5186	0.0330	1.6320	178.7	2.6408			
PTA–H_2O					0.0311/0.0204	1.7021/1.8723	158.1/141.8	2.6634/2.7191			
PTA–NH_3					0.0541	1.6604	169.1		0.0035	2.3457	120.9
PTA–MA					0.0691	1.6110	170.2		0.0048	2.3538	120.4
PTA–DMA					0.0803	1.5804	170.7		0.0059	2.3267	121.6
PTA–TMA					0.0818	1.5792	178.8				

[a] $\Delta r(OH) = r_{dimer} - r_{monomer}$, is the OH bond length change in the complexation. [b] The distance of inter-molecular hydrogen bond. [c] The angle of inter-molecular hydrogen bond. [d] The two oxygen atoms contact distance in the hydrogen bond. [e] $\Delta r(NH) = r_{dimer} - r_{monomer}$, is the NH bond length change in the complexation.

membered ring with H_2O through a CO–H···O hydrogen bond and an O–H···O hydrogen bond. The bond length r(H···B) in hydrogen bonds has been employed as an indicator of the hydrogen bond strength. Clearly, the hydrogen bond distances of all the complexes could be ranked as follows in ascending order: SO–H···O < CO–H···O/N < NH···O. This indicates that the SO–H···O hydrogen bond was the strongest in the complexes. Gilli *et al.* identified the contact distance d(O···O) between two oxygen atoms in a hydrogen bond as an indicator of hydrogen bond strength.[36] In the same complexes in this study, the contact distance d(O···O) of the SO–H···O hydrogen bond was shorter than that of the CO–H···O hydrogen bond. These results confirm that the SO–H···O hydrogen bond was the strongest in the complexes. The CO–H···O/N hydrogen bond was stronger than the N–H···O hydrogen bonds.

3.2 Interaction energy

The calculated binding energy (BE), zero-point vibrational energy (ZPVE), enthalpy of formation ($\Delta H^{\theta}_{298\ K}$) and Gibbs free energy of formation ($\Delta G^{\theta}_{298\ K}$) for the complexes are summarized in Table 2. The calculated $\Delta G^{\theta}_{298\ K}$ values were −7.99, −7.39, −4.47, −7.48, and −7.35 kcal mol^{-1} for BA–SA, PAA–SA, PA–SA, mPA–SA, and PTA–SA, respectively. This result indicates that the aromatic acids had the similar reactivity to interact with sulfuric acid except for PA. Apart from those observed for PA, the $\Delta G^{\theta}_{298\ K}$ values calculated for aromatic acid–SA complexes were more negative than those calculated for the aromatic acid–NH_3/amine complexes, indicating that the aromatic acids were more likely to interact with SA. This may have been due to the presence of intra-molecular hydrogen bonds, so PA is different from the other aromatic acids. The interaction of PA with NH_3/amine produced a lower Gibbs free energy compared with that produced by the PA–SA cluster. The $\Delta G^{\theta}_{298\ K}$ values of the aromatic acid–NH_3/amine complexes were obviously quite similar. Among all aromatic acid–NH_3/amine clusters, apart from PAA-containing clusters, the aromatic acid–DMA clusters had the lowest Gibbs free energy and the aromatic acid–TMA complexes had the highest Gibbs free energy in most clusters. This result proves that the interaction of aromatic acids with DMA was much stronger than those with NH_3, MA,

Table 2 Binding energy (BE), zero-point vibrational energy (ZPVE), enthalpy of formation ($\Delta H^{\theta}_{298\ K}$) and Gibbs free energy of formation ($\Delta G^{\theta}_{298\ K}$) at 298.15 K and 1 atm for aromatic acid-containing complexes derived at the PW91PW91/6-311++G(3df,3pd) level. The Gibbs free energies also calculated at M06-2X/6-311++G(3df,3pd) level. Energy is given in kcal mol^{-1}

Conformer	BE[a]	ZPVE	$\Delta H^{\theta}_{298\ K}$	$\Delta G^{\theta}_{298\ K}$ (PW91PW91)	$\Delta G^{\theta}_{298\ K}$ (M06-2X)
BA–SA	−19.78	−19.26	−19.29	−7.99	−8.25
BA–H_2O	−11.84	−9.50	−10.27	−0.57	−0.30
BA–NH_3	−12.46	−10.70	−11.09	−2.12	−1.78
BA–MA	−13.47	−12.27	−12.24	−2.59	−2.05
BA–DMA	−13.82	−12.85	−12.63	−2.79	−0.98
BA–TMA	−13.23	−12.41	−12.09	−1.89	−3.51
PAA–SA	−19.43	−18.81	−18.89	−7.39	−7.41
PAA–H_2O	−11.76	−9.47	−10.80	0.77	−0.62
PAA–NH_3	−12.49	−10.69	−11.12	−2.03	−0.12
PAA–MA	−13.47	−12.28	−12.26	−2.72	−1.65
PAA–DMA	−13.87	−12.85	−12.68	−2.51	−1.45
PAA–TMA	−13.40	−12.40	−12.19	−1.31	−2.22
PA–SA	−16.46	−15.67	−15.57	−4.47	−5.26
PA–H_2O	−11.84	−9.73	−10.36	−0.84	−1.41
PA–NH_3	−14.81	−13.36	−13.70	−4.95	−4.06
PA–MA	−16.18	−15.36	−15.32	−5.86	−4.14
PA–DMA	−16.71	−16.34	−16.09	−6.41	−4.97
PA–TMA	−16.46	−16.34	−16.03	−5.64	−5.34
mPA–SA	−19.31	−18.75	−18.76	−7.48	−7.94
mPA–H_2O	−11.94	−9.63	−10.38	−0.64	−0.46
mPA–NH_3	−13.01	−11.29	−11.66	−2.73	−2.42
mPA–MA	−14.16	−13.02	−12.96	−3.40	−2.37
mPA–DMA	−14.52	−13.65	−13.39	−3.77	−3.07
mPA–TMA	−13.96	−13.18	−12.87	−2.38	−3.44
PTA–SA	−19.24	−18.67	−18.67	−7.35	−7.67
PTA–H_2O	−11.88	−9.58	−10.33	−0.64	−0.37
PTA–NH_3	−13.05	−11.34	−11.70	−2.80	−2.18
PTA–MA	−14.14	−13.00	−12.85	−3.25	−2.51
PTA–DMA	−14.51	−13.62	−13.39	−3.50	−1.41
PTA–TMA	−14.02	−13.36	−12.99	−3.09	−3.66

[a] BE corrected with ZPVE.

and TMA. All aromatic acid–H_2O complexes, except for PAA, had the similar $\Delta G^{\theta}_{298\ K}$ value; the $\Delta G^{\theta}_{298\ K}$ value of PAA–H_2O was slightly higher than those of the other aromatic acid–H_2O clusters. The negative value of BEs indicates that the cluster was stable. Therefore, based on the BE, we can conclude that the aromatic acid–SA complexes were the easiest to form, followed by the aromatic acid–DMA complexes. The enthalpy $\Delta H^{\theta}_{298\ K}$ of hydrogen bond formation is directly related to the stabilization energy of a complex.[37] When we considered enthalpy, we could observe that the calculated values were consistent with the Gibbs free energy values of the complexes.

We compared the Gibbs free energy values of the aromatic monocarboxylic acids (BA, PAA)–SA complexes with those of the aromatic dicarboxylic acid (mPA, PTA)–SA complexes; we observed that the presence of the two carboxyls had little effect on the complexation process. However, increasing the number of carboxyl groups influenced the interaction of aromatic acids with NH_3 or amines. For example, the $\Delta G^{\theta}_{298\ K}$ value of the mPA–TMA cluster was lower than that of the PAA–TMA cluster by up to 4.33 kcal mol^{-1}. The value of the Gibbs free energy value of the BA-containing complexes was slightly lower than that of the PAA-containing complexes, signifying that methyl had an inhibitory role in the complexation process. Considering the different positions of the two carboxyl groups, the $\Delta G^{\theta}_{298\ K}$ value of the PA–SA complex (−4.47 kcal mol^{-1}) was quite different from those of the mPA–SA (−7.48 kcal mol^{-1}) and PTA–SA (−7.35 kcal mol^{-1}) complexes. The reason is that the two carboxyl groups in the *ortho*-position could form an intra-molecular hydrogen bond. Therefore, the presence of the intra-molecular hydrogen bond had a negative effect on the interaction of the aromatic acids and SA. This is consistent with the investigation of Jonas *et al.*, no or weak presence of intra-molecular hydrogen bond can stabilize the sulfuric acid cluster.[38] However, the Gibbs free energy values derived for mPA–SA and PTA–SA were nearly the same. A possible reason is that, when the two carboxyl groups were in the *meta*-position and *para*-position, they were not sufficiently far apart to form an intra-molecular hydrogen bond. Therefore, only one carboxyl was involved in the hydrogen bond formation in both. For the PA–NH_3/amines complexes, the complexation process was different from the complexation of the aromatic acids and SA. The presence of intra-molecular hydrogen bonds had a positive

effect on the interaction of the aromatic acids and NH_3/amine. The Gibbs free energy value of PA–DMA was 6.41 kcal mol^{-1}, whereas mPA–DMA was −3.77 kcal mol^{-1}.

According to the investigation by Nadykto and Yu at the PW91PW91/6-311++G(3df,3pd) level,[39] the $\Delta G^{\theta}_{298\ K}$ values obtained for formic acid (HCOOH)–SA and acetic acid (CH_3-COOH)–SA were −6.44 and −7.46 kcal mol^{-1}, respectively. Xu *et al.* discussed the Gibbs free energy of a pyruvic acid (CH_3-COCOOH)–SA cluster at the PW91PW91/6-311++G(3df,3pd) level,[40] the value which was −4.17 kcal mol^{-1}. According to the calculation, the interaction between $CH_3COCOOH$ and SA was weaker than that between BA and SA. Although $CH_3COCOOH$ has a lower pK_a value, the fact indicated that the acidity of monocarboxylic acid was not directly related to its cluster formation ability with SA. Comparing the Gibbs free energy values of BA–SA and PAA–SA clearly revealed that, aromatic monocarboxylic acids were basically similar or more likely to interact with SA compared with linear monocarboxylic acids. Xu *et al.* also reported that the Gibbs free energy values of malic acid ($HOOCCHOHCH_2COOH$)–SA and tartaric acid (HOOC-CHOHCHOHCOOH)–SA were −7.46 and −7.82 kcal mol^{-1}, respectively, at the PW91PW91/6-311++G(3df,3pd) level.[40] Miao *et al.* observed that the $\Delta G^{\theta}_{298\ K}$ values derived for oxalic acid (HOOCCOOH)–SA was −5.38 kcal mol^{-1} at the PW91PW91/6-311++G(3df,3pd) level.[41] PA has a lower pK_a value compared with mPA and PTA, however, the Gibbs free energies of PA–SA are about 3 kcal mol^{-1} lower than mPA–SA and PTA–SA complexes. The pK_a value of HOOCCOOH is lower than mPA and PTA, the formation of mPA–SA and PTA–SA heterodimers are easier than that of HOOCCOOH–SA. These all suggests that the acid strength does not directly correlate with its ability to form clusters with SA. We can conclude that the aromatic dicarboxylic acids had similar abilities to interact with SA than did the linear dicarboxylic acid. These results indicate that the affinities of aromatic acids to the SA were similar than those of linear monocarboxylic/dicarboxylic acid into SA. Moreover, the Gibbs free energy values of HCOOH–NH_3, CH_3COOH–NH_3, and $CH_3COCOOH$–NH_3 were calculated to be −2.82, −2.35, and −0.96 kcal mol^{-1}, respectively.[39,40] For the dicarboxylic acids–NH_3 clusters, the $\Delta G^{\theta}_{298\ K}$ value of $HOOCCHOHCH_2COOH$–NH_3, HOOCCHOHCHOHCOOH–NH_3 and HOOCCOOH–NH_3 were −3.62, −5.41, and −5.14 kcal mol^{-1}, respectively.[40,42] Hence, aromatic acids have similar ability to interact with NH_3 compared with that of monocarboxylic/dicarboxylic acids which is consistent with that of atomatic acid–SA and monocarboxylic/dicarboxylic acid–SA. According to Xu *et al.* and Nadykto *et al.*,[43,44] the Gibbs free energy value for SA–H_2O, SA–NH_3, SA–MA, SA–DMA, and SA–TMA were −0.28, −7.77, −11.03, −11.38, and −10.56 kcal mol^{-1}, respectively. Aromatic acids–SA and SA–NH_3 clusters have a similar magnitude of Gibbs free energies. However, the interactions between aromatic acid and SA are weaker than those between SA and MA/DMA/TMA.

3.3 Calculated OH/NH-stretching vibrational frequencies

To clarify the variety classes and the strength of the different hydrogen bonds in the aromatic acid containing heterodimers, we used the red shift ($\Delta\tilde{\nu}$), which is the wavenumber difference between free and hydrogen bonded OH-/NH-stretching vibrational transitions ($\Delta\tilde{\nu} = \tilde{\nu}_{monomer} - \tilde{\nu}_{dimer}$), to determine the interaction of different types of hydrogen bonds.[45,46] The calculated OH- and NH-stretching fundamental transition wavenumbers and the red shifts with respect to the heterodimers are summarized in Table 3. The red shifts and the changes in the intra-molecular OH bond lengths in the PA complexes are presented in Table S2.†

The red shifts of the OH-stretching transitions of the SO–H···O hydrogen bonds of BA/PAA/mPA/PTA–SA were calculated to be within the range of 1336–1443 cm^{-1}, and their corresponding intensities were increased by 70–84 times compared with those of the monomers. For the PA–SA complex, the red shift of the OH-stretching transition was calculated to be 924 cm^{-1}, and the intensity was calculated to be 50 times stronger than those of the monomers. This result is consistent with the Gibbs free energy value. Regarding the CO–H···O/N hydrogen bonds, formed between BA/PAA/mPA/PTA and NH_3 or amines, the red shift of the OH-stretching transition was within 918–1431 cm^{-1}, and the intensity was increased by more than 7 times relative to those of the monomers. Thus, we could rank the hydrogen bonds according to their strength as follows: SO–H···O > CO–H···O/N > N–H···O. Additionally, the red shifts of the OH-stretching transition of the intra-molecular hydrogen bond in the PA-containing complexes were considerably smaller than those of the inter-molecular hydrogen bond, indicating that the inter-molecular O–H···O hydrogen bond was stronger than the intra-molecular O–H···O hydrogen bond.

3.4 Topological analysis

The AIM analysis serves as a tool to gain deep insights into the nature of hydrogen bond interactions. The AIM calculations were performed at the PW91PW91/6-311++G(3df,3pd) level according to the wavefunctions of the monomers and heterodimers. The AIM plots of all the heterodimers with bond critical points (BCPs), ring critical points (RCPs), and electron density paths are depicted in Fig. 2. The topological parameters, including electron density $\rho(r)$, Laplacian of electron density $\nabla^2\rho(r)$ at the BCPs, and changes in atomic charge Δq(H) at the H atom determined using the PW91PW91 method, are listed in Table 4. The AIM parameters for the intra-molecular hydrogen bonds of the PA complexes are presented in Table S3.†

For the aromatic acid–SA complexes, the electron densities $\rho(r)$ at the BCPs for SO–H···O and CO–H···O were within 0.0646–0.0903 and 0.0519–0.0536 a.u., respectively. The electron densities $\rho(r)$ at the BCPs for the CO–H···O and N–H···O hydrogen bonds were within the limits of 0.0597–0.0804 and 0.0134–0.1053 a.u., respectively, in the aromatic acid–NH_3/MA/DMA/TMA complexes. On the basis of the standard proposed by Koch and Popelier,[47] for a hydrogen bond, the electron density $\rho(r)$ is usually within 0.002–0.040 a.u.[47,48] Clearly, the aforementioned $\rho(r)$ of the hydrogen bonds considerably exceed the upper limit of electron density values. The reason may be that the aromatic acids and SA/H_2O/NH_3/MA/DMA/TMA had strong hydrogen bond interactions. The values derived for the $\nabla^2\rho(r)$ for SO–H···O and CO–

Table 3 SO–H/O–H/N–H stretching wavenumbers and red shifts (cm^{-1}) of aromatic acid-containing complexes computed at the PW91PW91/6-311++G(3df,3pd) level

	SO–H···O			O–H···O/N			N–H···O		
Conformer	$\tilde{\nu}$	$\Delta\tilde{\nu}^a$	$f_D/f_M{}^b$	$\tilde{\nu}$	$\Delta\tilde{\nu}^a$	$f_D/f_M{}^b$	$\tilde{\nu}$	$\Delta\tilde{\nu}^a$	$f_D/f_M{}^b$
BA–SA	2222	1443	84.1	3044	609	37.6			
BA–H_2O				3077/3372	576/451	12.9/18.5			
BA–NH_3				2725	928	7.3	3492	213	14.8
BA–MA				2513	1140	43.8	3483	19	16.2
BA–DMA				2369	1284	52.4	3378	76	194
BA–TMA				2349	1303	57.3			
PAA–SA	2284	1381	69.8	3035	599	47.5			
PAA–H_2O				3070/3383	564/440	11.3/14.5			
PAA–NH_3				2716	918	43.6	3493	21	13.2
PAA–MA				2498	1136	58.3	3482	19	14.8
PAA–DMA				2358	1276	68.3	3383	71	151
PAA–TMA				2341	1294	75.4			
PA–SA	2741	924	49.8	3018	626	34.5			
PA–H_2O				2982/3042	662/21	18.2/0.8			
PA–NH_3				2443	1201	34.4			
PA–MA				2114	1530	41.2			
PA–DMA				1828	1816	40.5			
PA–TMA				1745	1899	28.8			
mPA–SA	2313	1352	83.1	3029	624	29.8			
mPA–H_2O				3055/3394	597/429	11.5/17.0			
mPA–NH_3				2665	987	28.9	3494	20	14.9
mPA–MA				2432	1212	37.1	3483	18	16.0
mPA–DMA				2269	1383	44.5	3386	68	145
mPA–TMA				2241	1411	48.4			
PTA–SA	2329	1336	85.6	3027	624	18.2			
PTA–H_2O				3052/3404	599/419	6.9/16.6			
PTA–NH_3				2658	994	17.0	3495	19	14.7
PTA–MA				2422	1230	21.7	3483	19	16.9
PTA–DMA				2253	1399	25.8	3386	68	156
PTA–TMA				2220	1431	28.1			

^{a} $\Delta\tilde{\nu} = \tilde{\nu}_{monomer} - \tilde{\nu}_{dimer}$. ^{b} f_D/f_M stands for the increase of intensity during the complexation.

H···O hydrogen bonds in the aromatic acid–SA complexes, were within the ranges of 0.0704–0.0971 and 0.1065–0.1067 a.u., respectively. For the aromatic acid–NH_3/MA/DMA/TMA clusters, the $\nabla^2\rho(r)$ values obtained for the CO–H···O and N–H···O hydrogen bonds were in the range of from −0.0412 to 0.0617 and from 0.0442 to 0.0503 a.u., respectively. These values were almost within the range of Laplacian criteria (0.014–0.139 a.u.).[47,48]

3.5 Atmospheric implication

To explain the role of aromatic acids in the formation of heterodimers from aromatic acids with common nucleation precursors in the atmosphere, the mass-balance equation was used to evaluate the atmospheric implication. Take BA–SA cluster as an example, the [BA–SA] concentration can be expressed as follows:

$$[\mathrm{BA-SA}] = [\mathrm{BA}] \times [\mathrm{SA}]\, e^{-\frac{\Delta G}{RT}} \quad (1)$$

where [BA–SA], [BA], and [SA] are the atmospheric mixing ratios of BA–SA, BA, and SA, respectively. The mixing ratios in eqn (1) can be written out *e.g.* as $[\mathrm{SA}] = p(\mathrm{SA})/p^0$, where $p(\mathrm{SA})$ is the SA partial pressure, and $p^0 = 1$ atm is the reference pressure at which ΔG is computed. ΔG is the Gibbs free energy during the formation of the BA–SA cluster, R is the molar gas constant in $J\ (mol\ K)^{-1}$, and T is the temperature in K.

Eqn (1) reveals that the concentration of the BA–SA complex is related to the concentrations of BA and SA and the value of the Gibbs free energy for cluster formation. The concentrations of SA, H_2O, NH_3, MA, DMA and TMA in ambient atmosphere were approximately 1×10^7, 2.46×10^{14}, 1×10^{11}, 1×10^9, 1×10^9, and 1×10^9, respectively. The concentrations of BA, PAA, PA, mPA, and PTA were 1.05×10^3, 7.50×10^8, 4.16×10^1, 5.47×10^0, and 1.71×10^2 molecule per cm^3, respectively.[49–51] The concentrations of the complexes from dimerization of aromatic acid and common nucleation precursor calculated by the mass-balance equation are listed in Table 5. For a given aromatic acid, the aromatic acid–H_2O complexes had the highest concentrations in the ambient atmosphere, followed by the aromatic acid–SA, and aromatic acid–NH_3/DMA. When compared the concentration of aromatic acid–NH_3 and aromatic acid–DMA clusters, for a given aromatic acid, the concentration of aromatic acid–NH_3 heterodimer is higher than that of

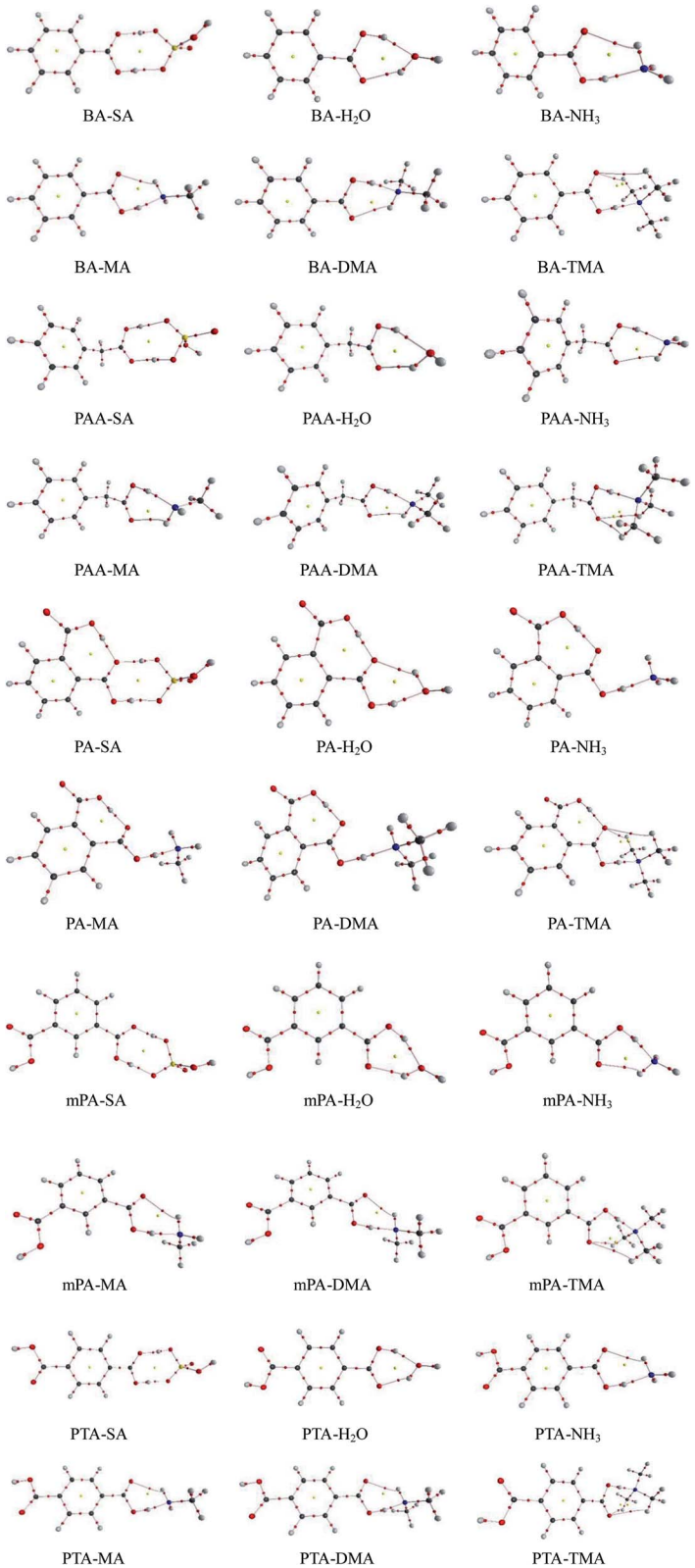

Fig. 2 Atom in molecules (AIM) graphs of aromatic acid-containing complexes obtained at the PW91PW91/6-311++G(3df,3pd) level. Red and yellow balls represent bond critical points (BCPs) and ring critical points (RCPs), respectively.

aromatic acid–DMA heterodimer. Thus, we can conclude that aromatic acid–H_2O complexes are abundant heterodimers due to the high concentration of water in the atmosphere. Owing to the lower Gibbs free energies of aromatic acid–SA/NH_3/DMA compared with that of aromatic acid–H_2O, they have a great possibility to form. Although the aromatic acid–

Table 4 Atoms in molecules (AIM) parameter analysis for aromatic acid-containing complexes calculated at the PW91PW91/6-311++G(3df,3pd) level. Units: a.u

	SO–H···O			O–H···O/N			N–H···O		
Conformer	$\Delta q(H)^a$	ρ^b	$\nabla^2\rho^c$	$\Delta q(H)^a$	ρ^b	$\nabla^2\rho^c$	$\Delta q(H)^a$	ρ^b	$\nabla^2\rho^c$
BA–SA	0.0396	0.0903	0.0704	0.0580	0.0524	0.1066			
BA–H_2O				0.0371/0.0551	0.2656/0.2037	0.1059/0.1010			
BA–NH_3				0.0198	0.0597	0.0169	0.0654	0.0147	0.0490
BA–MA				0.0116	0.0684	0.0481	0.0621	0.0145	0.0478
BA–DMA				0.0049	0.0740	0.0373	0.0596	0.0153	0.0503
BA–TMA				0.0045	0.0747	0.0319			
PAA–SA	0.0396	0.0871	0.0745	0.0604	0.0519	0.1065			
PAA–H_2O				0.0395/0.0554	0.2630/0.1976	0.1056/0.0993			
PAA–NH_3				0.0225	0.0598	0.0617	0.0636	0.0141	0.0464
PAA–MA				0.0137	0.0688	0.0477	0.0612	0.0140	0.0458
PAA–DMA				0.0078	0.0745	0.0365	0.0578	0.0144	0.0470
PAA–TMA				0.0072	0.0752	0.0313			
PA–SA	0.0414	0.0646	0.0971	0.0493	0.0536	0.1066			
PA–H_2O				0.0756/0.0531	0.0531/0.0227	0.1039/0.0790			
PA–NH_3				0.0076	0.0714	0.0430			
PA–MA				−0.0045	0.0856	0.0144			
PA–DMA				−0.0164	0.0996	−0.0218			
PA–TMA				−0.0214	0.1053	−0.0412			
mPA–SA	0.0395	0.0858	0.0779	0.0560	0.0529	0.1066			
mPA–H_2O				0.0359/0.0567	0.2721/0.1958	0.1059/0.0995			
mPA–NH_3				0.0173	0.0622	0.0584	0.0641	0.0138	0.0459
mPA–MA				0.0076	0.0719	0.0423	0.0606	0.0134	0.0443
mPA–DMA				0.0011	0.0787	0.0286	0.0574	0.0140	0.0460
mPA–TMA				0.0004	0.0796	0.0230			
PTA–SA	0.0401	0.0849	0.0791	0.0551	0.0531	0.1067			
PTA–H_2O				0.0358/0.0558	0.2732/0.1918	0.1059/0.0984			
PTA–NH_3				0.0179	0.0626	0.0578	0.0657	0.0134	0.0444
PTA–MA				0.0086	0.0723	0.0416	0.0607	0.0134	0.0442
PTA–DMA				0	0.0791	0.0277	0.0583	0.0141	0.0466
PTA–TMA				−0.0007	0.0804	0.0214			

[a] The change in atomic charge at the H atom. [b] The electron density at the BCPs. [c] The Laplacian electron density at the BCPs.

Table 5 Concentrations (molecule per cm^3) of the complexes from dimerization of aromatic acid and common nucleation precursor calculated by the mass-balance equation

Complexes	Concentrations	Complexes	Concentrations
BA–SA	2.98×10^{-4}	BA–MA	8.47×10^{-6}
BA–H_2O	1.59×10^{-2}	BA–DMA	1.19×10^{-5}
BA–NH_3	3.64×10^{-4}	BA–TMA	2.60×10^{-6}
PAA–SA	2.37×10^{2}	PAA–MA	7.41×10^{0}
PAA–H_2O	1.44×10^{3}	PAA–DMA	5.20×10^{2}
PAA–NH_3	2.31×10^{2}	PAA–TMA	6.85×10^{-1}
PA–SA	9.96×10^{-8}	PA–MA	8.84×10^{-5}
PA–H_2O	6.71×10^{-4}	PA–DMA	2.06×10^{-4}
PA–NH_3	1.93×10^{-3}	PA–TMA	5.32×10^{-5}
mPA–SA	2.08×10^{-6}	mPA–MA	1.70×10^{-7}
mPA–H_2O	6.50×10^{-5}	mPA–DMA	3.35×10^{-7}
mPA–NH_3	5.23×10^{-6}	mPA–TMA	3.15×10^{-8}
PTA–SA	5.50×10^{-5}	PTA–MA	4.51×10^{-6}
PTA–H_2O	2.16×10^{-3}	PTA–DMA	6.33×10^{-6}
PTA–NH_3	1.94×10^{-4}	PTA–TMA	3.17×10^{-6}

SA/NH_3/DMA has a lower concentration compared with that of aromatic acid–H_2O complexes, the role of SA, NH_3 and DMA in the dimerization cannot be ignored.

4. Conclusions

In summary, we theoretically investigated the molecular interaction between five aromatic acids (BA, PAA, PA, mPA, PTA) and some common atmospheric aerosol nucleation precursors. The following conclusions were drawn from the present study:

(1) The strength of the hydrogen bonds in aromatic acid-containing complexes could be ranked as follows in descending order: SO–H···O/N > CO–H···O/N > N–H···O hydrogen bonds.

(2) The BA/PAA/mPA/PTA–SA complexes had the lowest Gibbs free energy, followed by the BA/PAA/mPA/PTA-DMA complexes. For the PA-containing cluster, PA was more likely to interact with NH_3 or amines rather than SA.

(3) For the aromatic monocarboxylic acids, the presence of methyl impeded the complexation process. For the aromatic dicarboxylic acids, the two carboxyl groups in the *ortho*-position that formed an intra-molecular hydrogen bond promoted the interaction of NH_3 and amines, but hindered the interaction of SA. When the two carboxyl groups were in the *meta*-position and *para*-position, the extra carboxyl had little influence on the complexation.

(4) The aromatic monocarboxylic/dicarboxylic acids had similar abilities to interact with SA than did the linear monocarboxylic/dicarboxylic acids, apart from PA. The affinities of the linear monocarboxylic/dicarboxylic acids to NH_3 are similar compared with those of the aromatic acid–NH_3 complexes.

(5) The atomatic acid–H_2O clusters have the highest concentrations in the formation of heterodimers. Simultaneously, although the concentrations of aromatic acid–SA/NH_3/amine clusters are relatively a little low, they also have the potential to form during the formation of heterodimers owing to the relative low Gibbs free energies.

Conflicts of interest

There are no conflicts to declare.

Acknowledgements

This work was supported by NSFC (National Natural Science Foundation of China, project no. 91644214, 21677089, 21876102), Shenzhen Science and Technology Research and Development Funds (project no. JCYJ20160510165106371), FRFSDU (the Fundamental Research Funds of Shandong University, project no. 2016WLJH51, 2017JC033), the China Postdoctoral Science Foundation funded project (project no. 2017M612277, 2017T100493), SKLECRA (the open foundation of State Key Laboratory of Environmental Criteria and Risk Assessment, Chinese research academy of environmental sciences no. 2016OFP09).

References

1 R. Y. Zhang, *Science*, 2010, **328**, 1366–1367.
2 F. Q. Yu and G. Luo, *Atmos. Chem. Phys.*, 2009, **9**, 7691–7710.
3 P. Paasonen, A. Asmi, T. Petäjä, M. K. Kajos, M. Äijälä, H. Junninen, T. Holst, J. P. Abbatt, A. Arneth and W. Birmili, *Nat. Geosci.*, 2013, **6**, 438–442.
4 F. Q. Yu and A. G. Hallar, *J. Geophys. Res.: Atmos.*, 2014, **119**(12), 246–255.
5 R. Y. Zhang, A. Khalizov, L. Wang, M. Hu and W. Xu, *Chem. Rev.*, 2011, **112**, 1957–2011.
6 S. Ball, D. Hanson, F. Eisele and P. McMurry, *J. Geophys. Res.: Atmos.*, 1999, **104**, 23709–23718.
7 F. Q. Yu and R. P. Turco, *J. Geophys. Res.: Atmos.*, 2001, **106**, 4797–4814.
8 S.-H. Lee, J. Reeves, J. Wilson, D. Hunton, A. Viggiano, T. Miller, J. Ballenthin and L. Lait, *Science*, 2003, **301**, 1886–1889.
9 R. Y. Zhang, I. Suh, J. Zhao, D. Zhang, E. C. Fortner, X. X. Tie, L. T. Molina and M. J. Molina, *Science*, 2004, **304**, 1487–1490.
10 J. Zheng, A. Khalizov, L. Wang and R. Y. Zhang, *Anal. Chem.*, 2010, **82**, 7302–7308.
11 T. Nieminen, H. E. Manninen, S.-L. Sihto, T. Yli-Juuti, R. L. Mauldin, T. Petaja, I. Riipinen, V.-M. Kerminen and M. Kulmala, *Environ. Sci. Technol.*, 2009, **43**, 4715–4721.
12 R. Weber, P. H. McMurry, R. Mauldin, D. Tanner, F. Eisele, A. Clarke and V. Kapustin, *Geophys. Res. Lett.*, 1999, **26**, 307–310.
13 A. Chebbi and P. Carlier, *Atmos. Environ.*, 1996, **30**, 4233–4249.
14 J. Duplissy, P. F. DeCarlo, J. Dommen, M. R. Alfarra, A. Metzger, I. Barmpadimos, A. S. Prevot, E. Weingartner, T. Tritscher and M. Gysel, *Atmos. Chem. Phys.*, 2011, **11**, 1155–1165.
15 I. G. Kavouras, N. Mihalopoulos and E. G. Stephanou, *Nature*, 1998, **395**, 683.
16 W. F. Rogge, L. M. Hildemann, M. A. Mazurek, G. R. Cass and B. R. Simoneit, *Environ. Sci. Technol.*, 1993, **27**, 636–651.
17 I. Suh, R. Y. Zhang, L. T. Molina and M. J. Molina, *J. Am. Chem. Soc.*, 2003, **125**, 12655–12665.
18 M. Jang and S. R. McDow, *Environ. Sci. Technol.*, 1997, **31**, 1046–1053.
19 K. Kawamura and K. Ikushima, *Environ. Sci. Technol.*, 1993, **27**, 2227–2235.
20 T. Kleindienst, M. Jaoui, M. Lewandowski, J. Offenberg and K. Docherty, *Atmos. Chem. Phys.*, 2012, **12**, 8711–8726.
21 M. Fraser, G. Cass and B. Simoneit, *Environ. Sci. Technol.*, 2003, **37**, 446–453.
22 J. J. Schauer, M. J. Kleeman, G. R. Cass and B. R. Simoneit, *Environ. Sci. Technol.*, 1999, **33**, 1578–1587.
23 Y. F. Zhang, Y. Ma, L. Qi, Z. Wang, L. P. Wang and L. Zhu, *Environ. Sci.*, 2016, **37**, 2436–2442.
24 C. G. Liu and C. H. Zeng, *Chemosphere*, 2018, **209**, 560–567.
25 K. Kawamura and I. R. Kaplan, *Environ. Sci. Technol.*, 1987, **21**, 105–110.
26 W. Xu and R. Y. Zhang, *J. Phys. Chem. A*, 2012, **116**, 4539–4550.
27 J. R. Lane, J. Contreras-García, J.-P. Piquemal, B. J. Miller and H. G. Kjaergaard, *J. Chem. Theory Comput.*, 2013, **9**, 3263–3266.
28 R. Parthasarathi, V. Subramanian and N. Sathyamurthy, *J. Phys. Chem. A*, 2006, **110**, 3349–3351.
29 J. Zhang and M. Dolg, *Phys. Chem. Chem. Phys.*, 2015, **17**, 24173–24181.
30 J. Zhang and M. Dolg, *Phys. Chem. Chem. Phys.*, 2016, **18**, 3003–3010.
31 M. J. Frisch, G. W. Trucks, H. B. Schlegel, G. E. Scuseria, M. A. Robb, J. R. Cheeseman, G. Scalmani, V. Barone, B. Mennucci and G. A. Petersson, *Gaussian 09, revision A.02*, Gaussian, Inc., Wallingford, CT, USA, 2009.
32 J. Elm, M. Bilde and K. V. Mikkelsen, *J. Chem. Theory Comput.*, 2012, **8**, 2071–2077.
33 H. R. Leverentz, J. I. Siepmann, D. G. Truhlar, V. Loukonen and H. Vehkamaki, *J. Phys. Chem. A*, 2013, **117**, 3819–3825.
34 H. J. Zhang, O. Kupiainen-Määttä, X. H. Zhang, V. Molinero, Y. H. Zhang and Z. S. Li, *J. Chem. Phys.*, 2017, **146**, 184308.
35 R. F. Bader, *Chem. Rev.*, 1991, **91**, 893–928.
36 P. Gilli, V. Bertolasi, V. Ferretti and G. Gilli, *J. Am. Chem. Soc.*, 1994, **116**, 909–915.
37 L. Curtiss and M. Blander, *Chem. Rev.*, 1988, **88**, 827–841.
38 J. Elm, N. Myllys and T. Kurtén, *J. Phys. Chem. A*, 2017, **121**, 4578–4587.

39 A. B. Nadykto and F. Q. Yu, *Chem. Phys. Lett.*, 2007, **435**, 14–18.
40 Y. S. Xu, A. B. Nadykto, F. Q. Yu, J. Herb and W. Wang, *J. Phys. Chem. A*, 2009, **114**, 387–396.
41 S.-K. Miao, S. Jiang, J. Chen, Y. Ma, Y.-P. Zhu, Y. Wen, M.-M. Zhang and W. Huang, *RSC Adv.*, 2015, **5**, 48638–48646.
42 X.-Q. Peng, Y.-R. Liu, T. Huang, S. Jiang and W. Huang, *Phys. Chem. Chem. Phys.*, 2015, **17**, 9552–9563.
43 W. Xu and R. Y. Zhang, *J. Chem. Phys.*, 2013, **139**, 064312.
44 A. B. Nadykto, F. Q. Yu, M. Jakovleva, J. Herb and Y. S. Xu, *Entropy*, 2011, **13**, 554–569.
45 Q. Zhang and L. Du, *Comput. Theor. Chem.*, 2016, **1078**, 123–128.
46 L. Du and H. G. Kjaergaard, *J. Phys. Chem. A*, 2011, **115**, 12097–12104.
47 U. Koch and P. L. Popelier, *J. Phys. Chem.*, 1995, **99**, 9747–9754.
48 S. J. Grabowski, *J. Phys. Org. Chem.*, 2004, **17**, 18–31.
49 R. Y. Zhang, A. Khalizov, L. Wang, M. Hu and W. Xu, *Chem. Rev.*, 2011, **112**, 1957–2011.
50 F. Riccobono, S. Schobesberger, C. E. Scott, J. Dommen, I. K. Ortega, L. Rondo, J. Almeida, A. Amorim, F. Bianchi and M. Breitenlechner, *Science*, 2014, **344**, 717–721.
51 X. Ge, A. S. Wexler and S. L. Clegg, *Atmos. Environ.*, 2011, **45**, 524–546.